Eur. Phys. J. B **67**, 71–75 (2009)
DOI: 10.1140/epjb/e2009-00003-1

THE EUROPEAN PHYSICAL JOURNAL B

Regular Article

Curvature and external electric field effects on the persistent current in chiral toroidal carbon nanotubes

N. Xu[a], J.W. Ding[b], H.B. Chen, and M.M. Ma

Department of Physics & Institute for Nanophysics and Rare-earth Luminescence, Xiangtan University, Xiangtan, 411105, Hunan, P.R. China

Received 24 September 2008 / Received in final form 9 December 2008
Published online 9 January 2009

Abstract. Taking into account the intrinsic curvature, we calculate the persistent currents (I_{pc}s) in chiral toroidal carbon nanotubes (TCNs) by developing the supercell approach. It is shown that in the presence of curvature, the typical current (I_{ty}) oscillates with the unit cell number (P) and tends to be zero, while it damps exponentially in the absence of curvature. Due to the curvature effects, especially, a paramagnetism-diamagnetism transition is observed in chiral TCNs, depending on the ring diameter and chirality. In addition, the effect of external electric field energy (E_{ef}) on persistent current is also explored. It is shown that in the presence of electric field, I_{ty} vary unmonotonously with E_{ef}. A pronounced peak of I_{ty} is obtained at high E_{ef} region. By modulating the value of E_{ef}, a paramagnetism-diamagnetism or diamagnetism- paramagnetism transition is observed.

PACS. 73.23.Ra Persistent currents – 73.22.-f Electronic structure of nanoscale materials: clusters, nanoparticles, nanotubes, and nanocrystals

1 Introduction

A toroidal carbon nanotube (TCN) could be formed when a straight carbon nanotube (CN) was bent into the form of torus, satisfying simultaneously transversal and longitudinal periodical boundary conditions. This quasi-zero-dimensional TCN system was firstly observed by Liu et al. [1] and was synthesized in the gross [2]. These closed ring structures may be used as building blocks of small electromagnetic devices. For such applications, TCNs have attracted a lot of studies on their electronic and transport properties [3–30]. Of special interest is its persistent current (I_{pc}) [11–14] and magnetic response [18–20].

The geometric structure of TCNs determines the electronic structure and thus the persistent current. Such a current is caused by the magnetic flux ϕ through TCNs. Some works have been reported on this subject. In the absence of Zeeman splitting, Lin et al. [11] calculated the persistent current in TCNs by using Brillouin-zone (BZ) folding technique, where only one electron per site is kept and a constant hopping γ_0 is assumed between the first neighboring sites. It was shown that a metallic TCN will give rise to a paramagnetic moment, while a semiconducting TCN will yield a diamagnetic moment. At selected radii (magic radii), especially, an unusually large paramagnetic moment was obtained by Liu et al. [12], which was attributed to the interplay between the toroidal geometry and the ballistic motion of the electrons in TCN. By the extension of such a simple torus model, Latil [13] further studied the interacting nanotori and self-interacting coiled nanotubes. From the same model above, in addition, the electronic energy spectra and persistent currents of TCNs were studied theoretically in the presence of external fields and deformations. It is noticed that except for quantum wave vector, the curvature effect was not considered in such BZ folding models [11–16]. Considering only the curvature along transverse direction (Lin's model), Lin et al. [17] calculated the persistent currents in TCNs in the presence of Zeeman splitting. It was shown that most of armchair TCNs is diamagnetic while chiral TCNs are either paramagnetic or diamagnetic. Here, the curvatures along longitude direction were neglected. In a finite sized TCN, the curvatures are much more complicated than that of the corresponding straight CN. Unlike the perfect CNs, the local bond characteristic of the torus inner-side differs from that of the torus outer-side, which may lead to more complicated misorientation and rehybridization of the orbitals due to high curvature [10]. Therefore, one can expect that the curvature along longitude directions has pronounced effects on the electronic structure and thus on the persistent current in TCNs.

In previous works, theoretical simulations often focus mainly on the armchair and zigzag TCNs having the highest symmetry. There were few, if any, works reported on persistent current in chiral TCNs, especially in the case

[a] e-mail: nxu@xtu.edu.cn
[b] e-mail: jwding@xtu.edu.cn

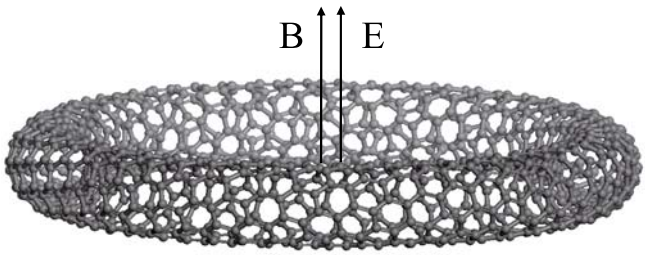

Fig. 1. Schematic view of the perpendicular-field configurations in the discussion.

of considering the curvature effects [11,14]. This may be since the atom number of a unit cell is very large even for a relatively small-diameter chiral TCN. Another reason is that there exist the complicated bond structures in chiral TCNs. It is a challenge to incorporate the curvatures along not only the transverse but also longitudinal directions into the study of persistent current in chiral TCNs [10,18,31].

In addition, the effects of electric and magnetic field on electronic structure of TCNs have been explored within tight-binding model [8,32]. It is shown that both the electric and magnetic field play an important role in determining electronic energy spectra. By changing electric field energy and magnetic field intensity, metal-insulator transitions are observed. Therefore, one expects that both of them have pronounced effects on the persistent currents in TCNs. In this paper, we consider both the electric and magnetic field applied perpendicularly to the torus plane, which is shown in Figure 1.

By developing the supercell approach [18], we calculate effectively the persistent currents in TCNs of various chirality, for which the curvatures along both the transverse and longitudinal directions are fully taken into account. It is shown that in the presence of curvature, the typical current oscillates with the unit cell number and tends to be zero, while it damps exponentially in the absence of curvature. Due to the curvature, especially, a paramagnetism-diamagnetism transition is observed in chiral TCNs, depending on the ring diameter and chirality. Additionally, it is shown that in the presence of electric field, I_{ty} vary unmonotonously with E_{ef}. A pronounced peak of I_{ty} is obtained at high E_{ef} region. By changing the value of E_{ef}, a paramagnetism-diamagnetism or diamagnetism-paramagnetism transition is observed. The results can provide a much better understanding of the transport properties of TCN as well as a typical way to describe similar structures.

2 Model and method

The tight-binding model with one π-electron per atom is very useful for describing the electronic structures of graphene, CNs, and TCNs [18]. In this study, we use this model to investigate electronic structure and persistent current in various TCNs. The tight-binding Hamiltonian may be written as

$$H = \sum_i \varepsilon_i \, c_i^+ c_i + \sum_{i,j} f(r_{ij}) \gamma_0 \exp(i\varphi_{i,j}) c_i + c_j, \qquad (1)$$

with ε_i the on-site potential. To consider the variations of bond length, the constant hopping parameter γ_0 between the first neighbor sites is multiplied by a modified factor $f(r_{i,j})$ [29]. The value of $\gamma_{i,j}$ is the bond-length between the sites i and j. $\{c_i^+, c_j\}$ are the creation and annihilation operators at site i and j. In our model, ε_i is set to be zero and hopping parameter $\gamma_0 = -3.00$ eV [8]. Based on the London approximation, the hopping integral between sites i and j are modified by a phase factor $(\exp(i\varphi_{i,j}))$ due to the presence of magnetic flux.

Within the adopted tight-binding approximation, the effect of the electric field is included in the on-site energies of carbon atoms in the Hamiltonian. The electric field energy in the sample is not calculated self-consistently and we simply assume a linear drop along the torus axis [32].

Following the notation of [13], we take the index (n, m, p) to define a TCN, formed from a finite length CN (n, m) containing p unit cells. We divide averagely the p unit cells into K supercells. In terms of the rotational symmetry, the effective Hamiltonian of a supercell is given by [10,15]

$$H_{eff} = H_0 + e^{i\beta} H_1 + e^{-i\beta} H_1^+, \qquad (2)$$

where H_0 and H_1 refer to the Hamiltonian matrix in the supercell and the coupling matrix between the two neighboring supercells, respectively. Here $\beta = j \times 2\pi/K$, $(j = 1, 2, 3, \ldots, K)$ is the phase difference between the wave functions of two neighboring supercells, where K is the number of the supercells contained in the system. For a given β, the eigenlevels can be obtained by diagonalizing the matrix H_{eff}. We have validated through comparing the results for the small sized TCNs with those obtained from directly diagonalizing the total Hamiltonian.

For noninteracting electrons, the total current of a nanotorus is calculated by the following expression [13]:

$$I_{pc}(T) = -\frac{1}{\Phi_0} \sum_n \frac{\partial \varepsilon_n}{\partial \phi}, \qquad (3)$$

where $\phi = \Phi/\Phi_0$ is the reduced flux with $\Phi_0 = h/e$ the flux quantum, ε_n is the eigenlevel of nanotorus. The current is a periodic function of ϕ with fundamental period Φ_0. Usually, one is interested in the typical current [13],

$$I_{typ} = \sqrt{\langle I^2 \rangle_\phi}, \qquad (4)$$

which is defined as the square root of flux average of the square of the persistent current.

3 Electronic structure and persistent current

Let us focus on the primary metallic chiral TCNs, in which there exists a larger persistent current. Such TCNs can be

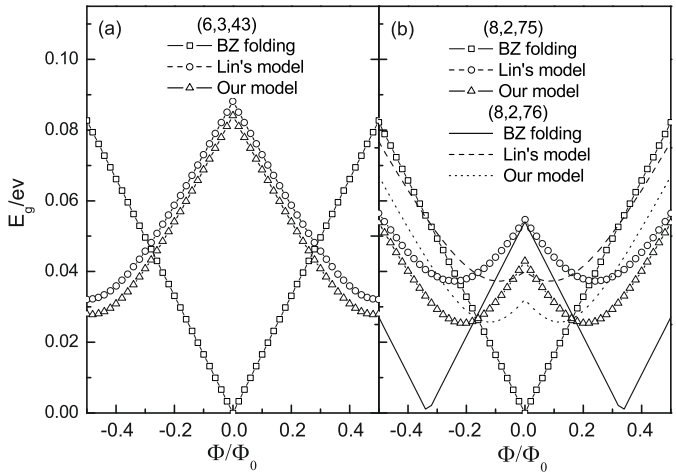

Fig. 2. The energy gaps of chiral TCNs versus flux. (a) metal-1 (6, 3, 43) TCN. (b) metal-2 (8, 2, 75) and (8, 2, 76) TCN.

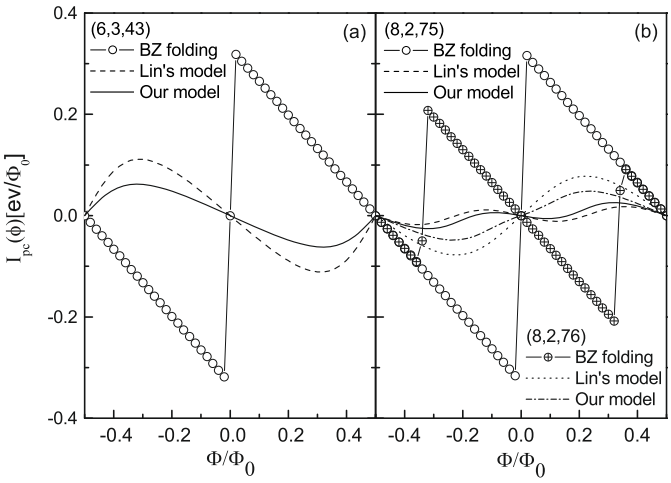

Fig. 3. The persistent currents of chiral TCNs are shown at $T = 0$. (a) metal-1 (6, 3, 43) TCN. (b) metal-2 (8, 2, 75) and (8, 2, 76) TCN.

classified into two general categories [12], depending on whether $n-m$ is multiple of $3d$ (metal-1) or not (metal-2), whenever $n-m$ is a multiple of 3. Here d is the highest common divisor of n and m.

Results for the energy gaps (E_gs) of chiral TCNs are shown in Figure 2. To facilitate comparisons of E_gs among chiral TCNs, we only focus on the chiral (6, 3, 43), (8, 2, 75) and (8, 2, 76) TCNs, which have almost the same torus-radius. For the type of metal-1, Figure 2a illustrates the E_g of chiral (6, 3, 43) TCN as a function of the magnetic flux. In the absence of curvature (BZ folding), a zero E_g exists at zero flux, indicating a magnetic flux induced metal-semiconductor transition. In the presence of the transverse curvature (Lin's model), obviously, there appears a nonzero energy gap, $E_g = 0.088$ eV in (6, 3, 43) TCN. Take into account both the transverse and longitudinal curvatures (our model), E_g decreases from 0.088 eV to be 0.084 eV. For the type of metal-2, we show E_gs of chiral (8, 2, 75) and (8, 2, 76) TCNs in Figure 2b. In the absence of curvature, E_g of (8, 2, 75) TCN exhibits a symmetrical 'V'-shaped curve as a function of flux, while a symmetrical 'W'-shaped curve emerges for the (8, 2, 76) TCN. It is shown that zero energy gap exists at $\Phi_c = i\Phi_0$ (i is an integer) for (8, 2, 75) TCN and at $\Phi_c = (i \pm 1/3)\Phi_0$ for (8, 2, 76) TCN. In the presence of the transverse curvature alone, $E_g = 0.054$ eV for (8, 2, 75) TCN, larger than 0.040 eV for (8, 2, 76) TCN, indicating a strong dependence of the electronic structure on ring diameter. In the presence of both the transverse and longitudinal curvatures, E_gs are decreased to be 0.043 eV and 0.032 eV in (8, 2, 75) and (8, 2, 76) TCNs, respectively. The results show that the longitudinal curvature has pronounced effects on the electronic structure, which can not be neglected to explore the persistent current of TCNs.

In Figure 3, we show the persistent currents (I_{pc}s) of chiral TCNs versus the magnetic flux within a period Φ_0. For the type of metal-1, the I_{pc} of (6, 3, 43) TCN versus the magnetic flux is shown. In the absence of curvature, the sawtooth shape of I_{pc} in (6, 3, 43) TCN changes abruptly at $\Phi_c = i\Phi_0$ (i is an integer). The discontinuous jump just corresponds to the metal-semiconductor transition, indicated in Figure 2a. For a metal-1 TCN, the energy spectrum is symmetric about E_F, thus $E_g = 2\varepsilon_m$ with ε_m being the energy of the highest occupied states. Therefore, $I_{pc} \approx -4[\partial\varepsilon_m/\partial\Phi]_{\Phi=0} \approx 2[\partial E_g/\partial\Phi]_{\Phi=0}$ is applicable. The factor 4 is due to the fact that there are four electrons occupying the highest occupied states. So a singularity can be derived at $\Phi_c = i\Phi_0$ from E_g–Φ curves in Figure 2a. In the presence of the transverse curvature alone, the (6, 3, 43) TCN is the narrow-gap semiconductor, and the sawtooth shape of persistent current is disappeared. The curve of I_{pc} fits well to $I = \pm A\sin(2\pi\Phi/\Phi_0)$. As can be seen from Figure 3a, the amplitude A of I_{pc} is obtained to be 0.11 eV/Φ_0, and a paramagnetism-diamagnetism transition is observed. In the presence of both the transverse and longitudinal curvatures, the amplitude A of I_{pc}s of (6, 3, 43) TCN decreases from 0.11 to 0.062 eV/Φ_0.

For the type of metal-2, the I_{pc}s of chiral (8, 2, 75) and (8, 2, 76) TCNs are shown in Figure 3b. It is shown that in the absence of curvature, the sawtooth shape of I_{pc} in chiral (8, 2, 75) TCN changes abruptly at $\Phi_c = i\Phi_0$ (i is an integer), while it changes abruptly at $\Phi_c = (i \pm 1/3)\Phi_0$ in chiral (8, 2, 76) TCN. These discontinuous jumps just correspond to the metal-semiconductor transition. With considering the transverse curvature alone, a paramagnetism-diamagnetism transition was observed in (8, 2, 75) TCN, while a diamagnetism-paramagnetism transition in (8, 2, 76) TCN. The effect of transverse curvature smooths the sawtooth shapes of I_{pc}s. In Figure 3b, the amplitude of I_{pc}s decreases from 0.32 eV/Φ_0 to 0.018 eV/Φ_0 for (8, 2, 75) TCN and from 0.21 eV/Φ_0 to 0.078 eV/Φ_0 for (8, 2, 76) TCN. In the presence of both the transverse and longitudinal curvature, interestingly, the amplitude of I_{pc} increases from 0.018 eV/Φ_0 to 0.026 eV/Φ_0 for (8, 2, 75) TCN and decreases from 0.078 eV/Φ_0 to 0.048 eV/Φ_0 for (8, 2, 76) TCN. Therefore, it is shown that both the transverse and longitudinal curvature have a strong effect on

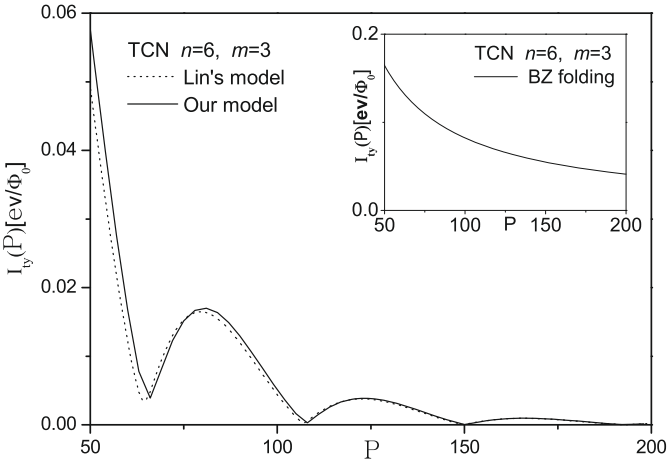

Fig. 4. The typical currents of chiral TCNs versus the unit cell number P. In the absence of curvature, the inset gives the typical current.

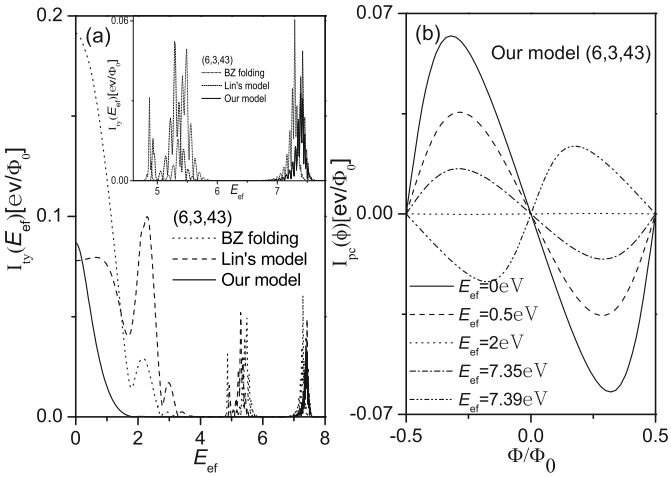

Fig. 5. (a) The typical currents dependence on the electric field intensity for (6, 3, 43) TCN. (b) The persistent currents vs. flux at various electric field energies.

not only the amplitude of I_{pc} but also the magnetic response, depending on the ring diameter and chirality.

To explore the torus size effect, in Figure 4a, we further calculate typical current (I_{ty}) as a function of the unit cell number (p). In this study, we focus on $(6, 3, p)$ TCN. In the absence of curvature, I_{ty} of $(6, 3, p)$ TCN decreases exponentially with p, as seen from the inset of Figure 4. In the presence of transverse curvature alone, the I_{ty} of $(6, 3, p)$ TCN exhibits an oscillatory behavior with p and tends to be zero, indicating the quantum size effect existing there, which is at variance with that in the absence of curvature. At a given $P = 50$, I_{ty} decreases from 0.164 eV/Φ_0 to 0.057 eV/Φ_0 due to the transverse curvature effect. In the presence of both the transverse and longitudinal curvature, a similar oscillatory curve is obtained. At $P = 50$, it is found that I_{ty} decreases to be 0.049 eV/Φ_0, which illustrate that the longitudinal curvature should be considered to explore the persistent current.

The external electric field alters the aspects of energy spectra and thus the persistent currents. In Figure 4a, I_{ty} versus E_{ef} is presented. In the absence of curvature, it is seen that I_{ty} vary unmonotonously with E_{ef}. At higher $E_{ef}(E_{ef} > 4$ eV), I_{ty} exhibits oscillation feature, with a series of isolated sharp peaks. At lower $E_{ef}(E_{ef} < 4$ eV), one can see that four peaks in I_{ty} profiles, superimposed on a smooth back ground. In the presence of transverse curvature alone, a similar I_{ty} curve is obtained. At lower E_{ef}, the value of I_{ty} is lower than that in the absence of curvature. In addition, three peaks are found in I_{ty} profiles. In the presence of both the transverse and longitudinal curvature, it is shown that at lower E_{ef}, I_{ty} decreases smoothly with E_{ef} and no peaks is found in I_{ty} curve. At higher E_{ef} (4 eV$< E_{ef} <$ 8 eV), only one pronounced peak superimposed on rapid oscillation feature is observed. The results show that the electric field effect strongly influence I_{ty}s. To further explore the effect of E_{ef} on persistent current, Figure 4b shows the persistent current versus flux at various E_{ef}. It is shown that the effect of electric field does not destroy the periodicity of the AB oscillation, which is remained to be Φ_0. Additionally, the curve of I_{pc} fits well to $I = \pm A\sin(2\pi\Phi/\Phi_0)$ with various E_{ef}. For $E_{ef} = 0$ eV, 0.5 eV, 7.39 eV, the (6, 3, 43) TCN exhibit diamagnetism at small ϕ, in which the values of A are obtained to be 0.062 eV/Φ_0, 0.035 eV/Φ_0, and 0.016 eV/Φ_0, respectively. However, for $E_{ef} = 2$ eV, 7.35 eV, the (6, 3, 43) TCN exhibit paramagnetism at small ϕ, in which the values of A are obtained to be 0.00013 eV/Φ_0 and 0.024 eV/Φ_0, respectively. Therefore, the persistent current of TCN can be modulated by the external electric field, which is helpful for the design and performance improvement of TCN molecular devices.

4 Conclusion

In summary, a reasonable and efficient supercell approach is developed to calculate the persistent current in chiral toroidal carbon nanotubes. The dependence of the persistent current on the torus size and the 'chirality' is investigated. It is shown that the high intrinsic curvature effects play an important role in determining the electronic structure and thus the persistent current of the novel nanostructure. Studies show that the magnetism of TCNs might change from diamagnetism into paramagnetism or paramagnetism into diamagnetism. In addition, it is shown that in the presence of curvature, the typical current exhibits oscillation feature with increasing the unit cell number and tends to be zero. In addition, the effect of external electric field energy on persistent current is also explored. A pronounced peak of I_{ty} is obtained at high E_{ef} region. By changing the value of E_{ef}, a paramagnetism-diamagnetism or diamagnetism- paramagnetism transition is observed. These results have implications for our understanding of magnetic properties and potential applications of TCN.

This work was supported by National Natural Science Foundation of China (No. 10674113), Program for New Century

Excellent Talents in University (NCET-06-0707), Foundation for the Author of National Excellent Doctoral Dissertation of China (Grant No. 200726), Scientific Research Fund of Hunan Provincial Education Department (No. 06A071), and partially by Hunan Provincial Innovation Foundation For Postgraduate (No. S2008yjscx06).

References

1. J. Liu, H. Dai, J.H. Hafner, D.T. Colbert, R.E. Smalley, S.J. Tans, C. Dekker, Nature **385**, 780 (1997)
2. R. Matel, H.R. Shea, P. Avouris, Nature **398**, 299 (1999)
3. M. Sano, A. Kamino, J. Okamura, S. Shinkai, Science **293**, 1299 (2001)
4. H.R. Shea, R. Martel, Ph. Avouris, Phys. Rev. Lett. **84**, 4441 (2000)
5. H. Watanabe, C. Manabe, T. Shigematsu, M. Shimizu, Appl. Phys. Lett. **78**, 2928 (2001)
6. M.F. Lin, R.B. Chen, F.L. Shyu, Solid State Commun. **107**, 227 (1998)
7. D-H. Oh, J.M. Park, K.S. Kim, Phys. Rev. B **62**, 1600 (2000)
8. A. Latgé, C.G. Rocha, L.A. Wanderley, M. Pacheco, P. Orellana, Z. Barticevic, Phys. Rev. B **67**, 155413 (2003)
9. Z.H. Zhang, Z.Q. Yang, X. Wang, J.H. Yuan, H. Zhang, M. Qiu, J.C. Peng, J. Phys.: Condens. Matter **17**, 4111 (2005)
10. C.P. Liu, J.W. Ding, J. Phys.: Condens. Matter **18**, 4077 (2006)
11. M.F. Lin, D.S. Chuu, Phys. Rev. B **57**, 6731 (1998)
12. L. Liu, G.Y. Guo, C.S. Jayanthi, S.Y. Wu, Phys. Rev. Lett. **88**, 217206 (2002)
13. S. Latil, S. Roche, A. Rubio, Phys. Rev. B **67**, 165420 (2003)
14. C.C. Tsai, F.L. Shyu, C.W. Chiu, C.P. Chang, R.B. Chen, M.F. Lin, Phys. Rev. B **70**, 075411 (2004)
15. R. Tamura, M. Ikuta, T. Hirahara, M. Tsukada, Phys. Rev. B **71**, 045418 (2005)
16. Z.H. Zhang, J.H. Yuan, M. Qiu, J.C. Peng, F.L. Xiao, J. Appl. Phys. **99**, 104311 (2006)
17. M.F. Lin, Physica B **269**, 43 (1999)
18. C.P. Liu, J.W. Ding, H.B. Chen, J. Phys.: Condens. Matter **20**, 015206 (2008)
19. M.F. Lin, J. Phys. Soc. Jpn **62**, 2218 (1998)
20. M.F. Lin, Phys. Rev. B **58**, 3629 (1998)
21. F.L. Shyu, Phys. Rev. B **72**, 045424 (2005)
22. H.R. Shea, R. Martel, Ph. Avouris, Phys. Rev. Lett. **84**, 4441 (2000)
23. H. Watanabe, C. Manabe, T. Shigematsu, M. Shimizu, Appl. Phys. Lett.**78**, 2928 (2001)
24. G. Cuniberti, J. Yi, M. Porto, Appl. Phys. Lett. **81**, 850 (2002)
25. Y.Y. Chou, G.-Y. Guo, L. Liu, C.S. Jayanthi, S.Y. Wu, J. Appl. Phys. **96**, 2249 (2004)
26. C.P. Liu, Z.X. Guo, J.W. Ding, X.H. Yan, Physica B **365**, 109 (2005)
27. J.F. Colomer, L. Henrard, E. Flahaut, G.V. Tendeloo, A.A. Lucas, P. Lambin, Nano Lett. **3**, 685 (2003)
28. H. Yu, Q.F. Zhang, G.H. Luo, F. Wei, Appl. Phys. Lett. **89**, 223106 (2006)
29. S. Froyen, W.A. Harrison, Phys. Rev. B **20**, 2420 (1979); W.A. Harrison, Phys. Rev. B **24**, 5835 (1981)
30. J.C. Charlier, P. Lambin, T.W. Ebbesen, Phys. Rev. B **58**, 54 R8377 (1996)
31. R. Tamura, M. Ikuta, T. Hirahara, M. Tsukada, Phys. Rev. B **71**, 045418 (2005)
32. C.G. Rocha, M. Pacheco, Z. Barticevic, A. Latgé, Phys. Rev. B **70**, 233402 (2004)